

Solvatochromism and Thermochemism of Fluconazole: An Experimental and Theoretical Study

Fernando G. Olivares,[✉]*^a Francisco G. Lazcano,^a Marcelo O. Castillo,^b
Maria G. Barúa,^a Juan P. Escalada^a and Graciela Pinto Vitorino^b

^aInstituto de Tecnología Aplicada, Unidad Académica Río Gallegos,
Universidad Nacional de la Patagonia Austral (ITA UARG UNPA),
Av. Piloto "Lero" Rivera y Av. Gdor. Gregores S/N, Río Gallegos, Santa Cruz, 9400, Argentina

^bGrupo Química Medicinal, Centro Regional de Investigación y Desarrollo Científico Tecnológico,
Facultad de Ciencias Naturales y Ciencias de la Salud,
Universidad Nacional de la Patagonia San Juan Bosco (GQM-CRIDEDECIT FCNyCS UNPSJB),
km 4, Comodoro Rivadavia, Chubut, 9000, Argentina

This research aims to study fluconazole (FNZ)-solvent interactions in pure solvents through theoretical and experimental solvatochromism. This study showed a bathochromic shift as the polarity of the solvent increases, where the excited state of FNZ is of higher polarity and lower energy than that of the ground state. The multiparametric statistical analysis highlighted solvent polarizability, dispersion, and electronic induction as solvent parameters of great importance, with the basicity of solvent and hydrogen bond acceptor capacity as having certain relevance. The thermochemic effect was also determined by exposing the three pK_a values of FNZ. In conclusion, this study shows the importance of the π - π stacking interaction of the FNZ dihalogenated phenyl ring, the solvent basicity for the hydroxyl group, and its acidity for the N4' of one of the triazoles stand out, as well as the acid-base equilibria involving the -OH group and the two N4'.

Keywords: fluconazole, solvatochromism, thermochemism, TD-DFT, multiparametric analysis

Introduction

Invasive fungal infections represent a serious and ever-present threat to human health and are associated with at least 1.5 million deaths worldwide each year. Due to their broad spectrum of activity, azoles (imidazoles and triazoles) are the most common antifungal drugs in clinical use. They bind to the cytochrome P450 (CYP51)-dependent enzyme lanosterol 14- α -demethylase in the cell membrane, encoded by the ERG11 gene, which converts lanosterol to ergosterol, thus inhibiting the growth and replication of fungi.¹⁻³

According to their date of discovery and subsequent structural modifications, the azoles are currently divided into four classes or generations. Second-generation triazoles, including fluconazole (FNZ) and itraconazole, exhibit a broader spectrum of antifungal activity compared

to imidazoles. In addition, they have significantly improved safety profiles and are generally well tolerated.^{1,2,4-6} Because it is one of the most widely used antifungal drugs and a better understanding of its physicochemical properties could lead to new therapeutic targets, we selected fluconazole for this study.

Also, there is a new successful approach to discovering effective drugs to treat several existing diseases through drug repositioning, which means the use of a drug in an indication other than the one for which it was initially marketed.⁷ Several drugs have been successfully repositioned to a new indication, with the most prominent being sildenafil and thalidomide, which have generated historically high revenues.⁸ More and more companies are scanning the existing pharmacopeia for repositioning candidates, and the number of repositioning success stories is increasing.⁹ FNZ, although an old triazole, could be a great candidate to be repositioned as a new therapeutic drug, as it has been shown the increasing interest in FNZ, voriconazole and itraconazole due to the pandemic disease

*e-mail: folivares@uarg.unpa.edu.ar

Editor handled this article: Paula Homem-de-Mello (Associate)

caused by severe acute respiratory syndrome coronavirus 2 (SARS-CoV-2) virus.¹⁰

Figure 1 shows the chemical structure of FNZ, 2-(2,4-difluorophenyl)-1,3-bis(1,2,4-triazole-1-yl)propan-2-ol.

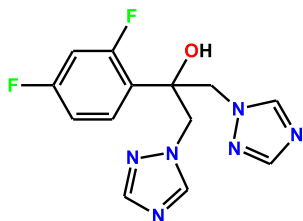


Figure 1. Chemical structure of the antifungal FNZ.

Active pharmaceutical ingredients (APIs) interact with multiple environments throughout the entire manufacturing process and subsequent assimilation by the body.¹¹ Therefore, it is essential to know the properties of APIs in different microenvironments to predict their pharmacokinetic and pharmacodynamic properties and to provide valuable information for all pharmaceutical steps.^{12,13}

It is known that the microenvironment of the solution that surrounds a solute molecule, or cybotactic region, exerts a great influence on its physicochemical properties. The modifications that occur in the absorption spectra for certain organic molecules, depending on the polarity characteristics of the environment, are known as the solvatochromic effect.^{12,14} Its analysis makes it possible to measure the difference between the ground state and the excited state of a molecule, where the solvent acts as a constant electric field applied to the solute in question, with an intensity directly proportional to the magnitude of its dielectric constant. The extent and direction of solvatochromism (bathochromic effect, positive or red solvatochromism: shift to longer wavelengths; hypsochromic effect, negative or blue solvatochromism: shift to shorter wavelengths) depends on how stable the structure of the solute is in the ground state and in the excited state.^{15,16} It is known that the conformation with the highest dipole moment is the most stable in solvents with a high dielectric constant.¹⁷

The presence of specific and non-specific interactions between the solvent and the solute molecules is responsible for the variation of the molecular geometry, the electronic structure, and the dipole moment of the solute.¹⁵⁻¹⁹

Thermochromism is the reversible transformation of a molecular structure or system, induced by changes in the temperature of a solution, liquid or solid, and which produces a spectral variation. The mechanism responsible for thermochromism varies with the molecular structure. This phenomenon can be caused by an equilibrium

between two molecular species (acid-base, keto-enol, lactim-lactam), a ring opening, a thermally accessible triplet state or the formation of free radicals, among others. Thermochromic studies are carried out by determining the absorbance of a solution at different temperatures. The generation of isosbestic points indicates the presence of an intermolecular equilibrium. If the spectra cross, but not all at the same point, that is, without isosbestic points, it can be interpreted that there are several simultaneous equilibria in the solution.²⁰⁻²²

The stability of the FNZ molecule has been extensively investigated through conformational studies, electronic delocalization, electrostatic potentials, and thermodynamic parameters, as well as the effect of some solvents on its UV-Vis absorption spectrum.^{19,23} Similarly, various polymorphs of FNZ have been analyzed in the crystalline state, proving its great conformational flexibility.²⁴

However, there is no evidence in the literature consulted of an analytical study that analyzes the interaction of solvents of different polarities with FNZ, nor its thermochromism at physiological pH.

In another way, theoretical approaches are common in the study of electronic structure to predict and understand the properties of molecular systems. A frequently used computational method is the density functional theory (DFT) which is based on the determination of the energy of an electronic state from the electronic density.²⁵ The free energy of solvation calculates the energy change in the transfer of a molecule from the gas to the solvent and is used to calculate a variety of properties such as activity coefficients and solubilities.²⁶ Although FNZ has already been studied with the functional Becke, 3-parameter, Lee-Yang-Parr (B3LYP) method, other bases introduce certain modifications, such as CAMB3LYP, a hybrid functional with improved long-range properties.^{19,27-30} In addition, the polarizable continuum model (PCM) is a method commonly used in computational chemistry to simulate the effects of solvation. While Integral Equation Formalism PCM (IEFPCM) is the current version of PCM that is applied in the usual quantum chemistry packages, the conductive polarizable continuum model (CPCM) variant of PCM is often considered one of the most popular successful solvation models.^{29,31}

DFT has introduced descriptors of global and local chemical reactivity. In the case of global descriptors, these provide information about the reactivity of the molecule and are calculated by using the Koopmans theorem, considering the energies of the frontier orbitals highest occupied molecular orbital (HOMO) and lowest unoccupied molecular orbital (LUMO).^{26,32} Some usual calculations to estimate the chemical reactivity

of a molecule are energy gap, hardness (η), chemical potential (μ), electrophilicity (ω), electrodonating, and electroaccepting power.^{33,34}

This research aims to study the solute-solvent interactions of the antimycotic azole FNZ in pure solvents through theoretical and experimental solvatochromism with multiparametric statistical analysis. The thermochemical effect on the UV-Vis spectrum in a buffer solution compatible with physiological pH is also determined. These two methodologies were not performed in the current published literature. The analysis of the physicochemical properties of FNZ may lead to a better understanding of its structural attributes and impact on biological action.^{29,30,35}

Experimental

Quality control and preparation of experimental samples

The API and solvents used were of the highest analytical purity. FNZ was purchased from Parafarm (Buenos Aires, Argentina), and all the reagents and solvents used for spectroscopic studies were of the commercially available highest grade (Parafarm, Buenos Aires, Argentina). The absorption spectra were obtained by using a Varian Cary 50 Conc UV-Vis spectrophotometer equipped with a Peltier thermostatic and a fiber optic system (Varian, Mulgrave, Victoria, Australia). The radiation source was a xenon lamp, and a 1 cm optical path quartz cuvette was used. For FNZ quality controls, the melting point was determined in triplicate with an Opti Melt MPA100 automatic melt meter applying a heating ramp of 1 °C min⁻¹ and a temperature range of 130 to 160 °C (Stanford Research System, Sunnyvale, California, USA). Additionally, analytical purity was determined by thin layer chromatography (TLC) and high-performance liquid chromatography (HPLC). For the TLC, a Merck silica gel 60 F254 aluminum plate (Darmstadt, Germany, Merck S. A.) and a mobile phase of chloroform-ethyl acetate-glacial acetic acid-water in a 4:4:4:1 ratio was used.³⁶ The HPLC was performed using a Shimadzu LC-20AT equipment with an SPD-M20A diode array UV-Vis detector (Kyoto, Japan, Shimadzu), a Phenomenex Gemini C18 column 150 mm long stationary phase of 4.6 mm internal diameter and a particle diameter of 5 μ m (Phenomenex, Torrance, California, USA). The mobile phase was a 19:81 acetonitrile-water solution at a flow rate of 0.5 mL min⁻¹. The preparation of FNZ samples was carried out by Argentinian Pharmacopoeia (FA) VII edition.³⁷ The quality of the solvents was verified by measuring the refractive index with a Reichert AR200 pocket digital refractometer (Leica, Deerfield, Illinois, USA).

The buffer solution was prepared according to the FA³⁸ using 0.2 M monobasic potassium phosphate solution and NaOH until a solution of pH 7.4 was achieved. It was validated with a JP Selecta pH-2005 digital benchtop pH meter (Mettler Toledo, Leicester, United Kingdom). The solvatochromic study of FNZ was carried out with 1.0×10^{-3} M solutions that comply with the Lambert-Beer law.¹⁹ Seven pure polar solvents, three protic (2-propanol (2-PrOH), ethanol (EtOH), methanol (MeOH)), and four aprotic (diethyl ether (DE), dichloromethane (DCM), acetonitrile (AcN), dimethyl sulfoxide (DMSO)) and a pH 7.4 buffer solution were used. The thermochemical study was carried out with a 1.0×10^{-3} M FNZ solution in a pH 7.4 buffer. All spectra were determined at 20.0 ± 0.1 °C. The experiments were performed in triplicate and average results were used for data analysis.

Solvatochromic and thermochemical studies

The distinction between specific and nonspecific solute-solvent interactions in the interpretation of experimental determinations of absorption spectra is difficult. Therefore, it is necessary to consider quantitative measures of polarity to differentiate between these two effects. Thus, several multiparametric equations have been developed that combine two or more solvent parameters to explain the particular and distinctive aspects of the solvent effect on a given compound,^{27,39-41} among them, those of Kamlet and Taft,^{12,13} Catalán⁴⁰ and Laurence⁴¹ are the most employed.

Regarding all existing solvent polarity scales, the empirical solvatochromic scale of Kamlet and Taft⁴²⁻⁴⁶ stands out, based on the linear solvation energy relationships (LSER).^{39,42-46}

The Kamlet and Taft⁴⁴ method rationalize the effect of the solvent in terms of a linear combination of three variables: the parameter π^* refers to the shared effect of the polarity-polarizability of the solvent, which measures the ability of the environment to stabilize the charges of a dipole due to its dielectric effects. This parameter relates to non-specific interactions. The parameter α describes the acidic capacity of the solvent to donate a proton through hydrogen bonding (HBD) and the parameter β measures the basic ability of the solvent to accept hydrogen bonds (HBA). The last two parameters imply specific interactions.⁴⁶

These solvatochromic parameters are related with the following equation:

$$A = A_0 + a\alpha + b\beta + s\pi^* \quad (1)$$

where A ($\bar{\nu}_{\max} = 1/\lambda / \text{cm}^{-1}$) is the property of the solute to be correlated; A_0 is the value of this property for the same

solute in the gas phase or in a hypothetical solvent for which $\alpha = \beta = \pi^* = 0$;^{13,44} a, b and s are the coefficients that calculate the relative susceptibility of A to the parameters already defined: α , β and π^* , respectively.

The Catalán⁴⁷ equation is an improvement in the multiparametric analysis concerning the Kamlet and Taft⁴⁵ equation.^{13,39,47} While the latter was made from data belonging to an average of around 40 determinations made by different authors in various laboratories, the former was created from data obtained in the same laboratory for pairs of homologous structures.⁴⁰

Both the Catalán SPP descriptor and the Kamlet and Taft π^* descriptor explain the polarity of the solvent, although the π^* parameter was obtained from π - π^* transitions of some azo dyes. The SPP descriptor was calculated from different transitions of many compounds. Even though multiparametric procedures have provided excellent results in the analysis of the effect of the solvent, there is also experimental evidence of some relevant deficiencies such as their inability to describe the solvatochromic behavior of nonpolar solutes that do not exhibit any specific interaction with the solvent.⁴⁷ Therefore, Catalán⁴⁷ separated the SPP polarity scale into two parameters: the solvent polarizability (SP) and dipolarity (SdP) scales, resulting in a four-parameter model.³⁹ According to this model, the specific interactions are described by the parameters SA, which shows the solvent acidity, and SB, which provides the measurement of the solvent basicity. Nonspecific interactions are now characterized by two independent parameters: SP and SdP. The equation is given by:

$$A = A_0 + a_{SA}SA + b_{SB}SB + c_{SP}SP + d_{SdP}SdP \quad (2)$$

where A ($\bar{\nu}_{\max} = 1/\lambda / \text{cm}^{-1}$) is the solvent-dependent physicochemical property in a given solvent; A_0 is the statistical quantity of the value of the property in the gas phase; SA, SB, SP and SdP, represent the independent parameters, although complementary, that account for solute-solvent interactions; a_{SA} , b_{SB} , c_{SP} and d_{SdP} are the regression coefficients that measure the relative susceptibility of to the different interaction forces.⁴⁷

On the other hand, the Laurence equation allows the estimation of the dispersion and electrostatic solute-solvent interactions of a given system with greater precision.^{39,41} It is based on both experimental measurements and theoretical calculations.³⁹ According to this model, the nonspecific intermolecular forces are determined by the DI parameter, which describes the dispersion and induction interactions, and the ES parameter, which describes the electrostatic interactions between the permanent multipoles of the solute and the solvent. While the specific interactions are described

by the parameter α_1 , which quantifies the solute HBA/solvent HBD interactions (the hydrogen-bond acidity of solvent); and the parameter β_1 , that accounts for the solute HBD/solvent HBA interactions (the hydrogen-bond basicity of solvents).⁴¹

This parametric analysis is determined by the equation:

$$A = A_0 + diDI + eES + a_1\alpha_1 + b_1\beta_1 \quad (3)$$

where A ($\bar{\nu}_{\max} = 1/\lambda / \text{cm}^{-1}$) is the property of the solute to be correlated, A_0 is the statistical quantity of the value of the property in the gas phase. DI, ES, α_1 and β_1 represent the independent, although complementary, parameters that account for solute-solvent interactions; di, e, a_1 and b_1 are the regression coefficients that evaluate the relative susceptibility of A to the different interaction relationships.^{27,41}

In solvatochromic and thermochromic studies, the UV-Vis absorption spectrum was measured from 225 to 325 nm, at a scanning speed of 1 nm s⁻¹. The solvatochromic samples were kept at a constant temperature of 20 °C for 5 min before the spectroscopic determination. The thermochromic samples were thermostated for 5 min before each determination, taking the data with a gradient of 5 °C in the temperature range between 5 and 75 °C. The $\bar{\nu}_{\max} / \text{cm}^{-1}$ of each spectrum was measured by taking the midpoint between two positions of the spectrum where the absorbance is equal to 0.9.^{22,45}

The results were analyzed by the Kamlet and Taft method, the Catalán method, and the Laurence method. The wavenumber of maximum absorption, $\bar{\nu}_{\max}$, was related to the empirical solvent parameters of Kamlet-Taft equation: α , β , π^* , Catalan equation: SA, SB, SP, SdP, and Laurence equation: DI, ES, α_1 , β_1 . The correlation study was carried out using multiparameter linear regression data analysis, taking $\bar{\nu}_{\max}$ as the dependent variable and the former parameters as independent variables (Table 1).

Geometric optimization, conformational analysis, and molecular descriptors

The FNZ structure was traced using Gaussview 5.0⁴⁸ software and optimized with geometric calculations using Gaussian 9.0 software.⁴⁹ Initially, the geometric optimization was carried out employing Molecular Mechanics universal force field (UFF) to obtain the most stable structure using the semi-empirical methods Austin Model 1 (AM1) and Parametric Method 3 (PM3).

The conformational analysis of FNZ reported by Chandrasekaran and Thilak Kumar¹⁹ evidenced the relevance of the dihedral angle C5–C10–O3–H32 (Figure 2). Rotation around the C5–C10 single bond produces different conformers of the molecule since

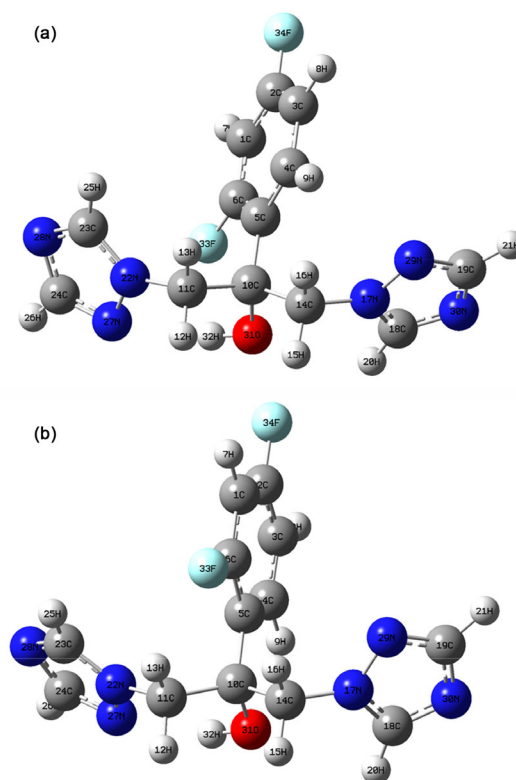
Table 1. Physical constants and empirical solvatochromic parameters of solvents

Solvent	$\mu\text{D}/\text{Debye}$	E_r	n_D	$\eta / (10^{-3} \text{ Pa s})$	Kamlet-Taft			Catalán				Laurence			
					π^*	α	β	SP	SdP	SA	SB	DI	ES	α_1	β_1
Cy	0.00	2.02	1.4262	0.89	0.00	0.00	0.00	0.683	0.000	0.000	0.073	0.78	0.00	0.00	0.00
Tet	0.00	2.24	1.4602	0.90	0.21	0.00	0.10	0.768	0.000	0.000	0.044	0.82	0.10	0.00	0.00
Ben	0.00	2.27	1.5011	0.60	0.55	0.00	0.10	0.793	0.270	0.000	0.124	0.87	0.23	0.00	0.14
DE	1.15	4.20	1.3524	0.22	0.27	0.00	0.47	0.617	0.385	0.000	0.562	0.68	0.26	0.00	0.58
DCM	1.36	8.93	1.4242	0.41	0.79	0.04	-0.01	0.761	0.769	0.040	0.178	0.78	0.60	0.10	0.00
AcN	3.92	35.94	1.3441	0.37	0.75	0.19	0.31	0.645	0.974	0.044	0.286	0.67	0.84	0.23	0.37
DMSO	3.98	46.45	1.4793	1.99	1.00	0.00	0.76	0.830	1.000	0.072	0.647	0.84	1.00	0.00	0.71
2PrOH	1.56	19.92	1.3772	2.04	0.48	0.76	0.84	0.633	0.808	0.283	0.830	0.71	0.77	0.53	0.68
EtOH	1.66	24.55	1.3614	1.07	0.54	0.83	0.77	0.633	0.783	0.400	0.658	0.69	0.80	0.75	0.62
MeOH	1.70	32.66	1.3284	0.54	0.60	0.93	0.62	0.608	0.904	0.605	0.545	0.64	0.84	1.00	0.54
Water	1.85	78.36	1.3330	0.89	1.09	1.17	0.47	0.681	0.997	1.062	0.025	0.65	0.89	1.54	0.37

Cy: cyclohexane; Tet: tetrachloromethane; Ben: benzene; DE: diethyl ether; DCM: dichloromethane; AcN: acetonitrile; DMSO: dimethyl sulfoxide; 2PrOH: 2-propanol; EtOH: ethanol; MeOH: methanol; μD : dipolar moment; E_r : dielectric constant; n_D : refractive index; η : viscosity at 25 °C; SP: solvent polarizability; SdP: dipolarity; π^* : polarity-polarizability of the solvent; α : the acidic capacity of the solvent; β : the basic capacity of the solvent; SA: solvent acidity; SB: solvent basicity; DI: dispersion and induction interactions; ES: electrostatic interactions; α_1 : hydrogen-bond acidity of solvent; β_1 : hydrogen-bond basicity of solvents.

C10 is attached to a hydroxyl group, a phenyl ring, and methylene groups. Hence, the conformational scan of the C6–C5–C10–O31 dihedral angle was performed, rotating the eclipsed phenyl ring with the C10–O31 bond every 15° in the range of 0–360° and calculating the potential energy of every conformation. Subsequently, the minimum energy of this conformational scan was selected and the dihedral angle C5–C10–O31–H32 was analyzed, varying the position of H32 every 15° in the range of 0–360° until a new minimum was obtained. The FNZ structure obtained was optimized by *ab-initio* methods HF/3-21+G*, HF/6-31+G(d), DFT-B3LYP/3-21+G*, DFT-B3LYP/6-31+G(d) and DFT-CAMB3LYP/6-31+G(d). Since the geometric structure found by the aforementioned authors¹⁹ was a conformer with the halogenated phenyl group in the opposite position to the hydroxyl group, this geometry was emulated by rotating it exactly 180° in relation to the initial molecule and optimized by semi-empirical methods.¹⁹ Then, optimizations were obtained by using the *ab-initio* methods already mentioned. Two slightly different FNZ conformers were obtained (Figure 2).

Frequency calculations were performed on the structures obtained by DFT-B3LYP and DFT-CAMB3LYP of FNZ conformers **I** and **II** to verify whether these conformations corresponded to energy minima according to their vibrational states. Next, the potential energy, the dipole moment, the wavelength of maximum absorbance, and the energies corresponding to the HOMO and LUMO frontier orbitals were calculated by Time-dependent self-consistent field (TD-SCF) methods both in a vacuum and in solvation sphere with the Conductor-like Polarizable

**Figure 2.** Chemical structure of the conformer **I** (a) and **II** (b) of the antifungal FNZ.

Continuum Model (CPCM), choosing ten solvents whose dipole moments are included in Gaussian.⁴⁹

Analysis of the geometric structures of FNZ conformers **I** and **II** was performed by measuring specific bond lengths, angles, and dihedral angles. They were compared with those described by Chandrasekaran and Thilak Kumar¹⁹ and some crystallized polymorphs of FNZ.^{19,24}

The global molecular descriptors hardness (η), chemical potential (μ), electronegativity (ω), electron-donating power (ω^-) and electron-accepting power (ω^+) were calculated using the Koopmans procedure in DFT, in which EA (electronic affinity) = $-E_{\text{LUMO}}$ and IE (ionization energy) = $-E_{\text{HOMO}}$, resulting in the following parameters:

$$\eta = \frac{(IE - EA)}{2} \approx \frac{E_{\text{LUMO}} - E_{\text{HOMO}}}{2} = \eta_{\text{K}} \quad (4)$$

$$\mu = \frac{-(IE + EA)}{2} \approx \frac{E_{\text{LUMO}} + E_{\text{HOMO}}}{2} = \mu_{\text{K}} = -\chi_{\text{K}} \quad (5)$$

$$\omega = \frac{\mu^2}{2\eta} \quad (6)$$

$$(\omega^-) = \frac{(3IE + EA)^2}{16(IE - EA)} \approx \frac{(3E_{\text{HOMO}} + E_{\text{LUMO}})^2}{16(E_{\text{LUMO}} - E_{\text{HOMO}})} = \omega_{\text{K}}^- \quad (7)$$

$$(\omega^+) = \frac{(IE + EA)^2}{16(IE - EA)} \approx \frac{(3E_{\text{HOMO}} + 3E_{\text{LUMO}})^2}{16(E_{\text{LUMO}} - E_{\text{HOMO}})} = \omega_{\text{K}}^+ \quad (8)$$

Theoretical solvatochromic study

Solvatochromic analysis of FNZ was performed at the theoretical maximum absorbance wavelengths obtained by DFT-B3LYP and DFT-CAMB3LYP of conformers **I** and **II**. For this, the multiparametric equations of Kamlet and Taft, Catalán, and Laurence were used. First, the same solvents used in the experimental study were chosen, whose dipole moments were included by default in Gaussian (it was excluded 2-PrOH and buffer pH 7.4 and was added water instead). Second, cyclohexane (Cy), tetrachloromethane (Tet), and benzene (Ben) were incorporated into the database to include the FNZ solvation effect in non-polar solvents, constituting a set of ten solvents. Finally, the relative contributions of the specific and non-specific interactions were compared in each case.

Results and Discussion

Geometric optimization, conformational analysis, and molecular descriptors

Conformational scanning of the C6–C5–C10–O31 (θ) and C5–C10–O31–H32 (φ) dihedral angles were performed, as well as the calculation of the potential energy of each FNZ conformer before molecular optimization by *ab-initio* methods. The energy minima were obtained with $\theta = 195^\circ$ and $\varphi = 135^\circ$ for conformer **I** and with $\theta = 0^\circ$ and $\varphi = 15^\circ$ for conformer **II**.

After geometric optimization, the potential energies in vacuum calculated at the DFT-B3LYP/6-31+G(d) level of the FNZ conformers were $E_{\text{I}} = -2,903,855.09 \text{ kJ mol}^{-1}$ and $E_{\text{II}} = -2,903,877.46 \text{ kJ mol}^{-1}$, while at the DFT-CAMB3LYP/6-31+G(d) level they were $E_{\text{I}} = -2,902,607.37 \text{ kJ mol}^{-1}$ and $E_{\text{II}} = -2,902,629.36 \text{ kJ mol}^{-1}$. It can be noted that the lowest potential energy minima were obtained with the B3LYP calculation method, instead of with CAMB3LYP.

The frequency analysis of the vibrational modes belonging to the optimized molecular geometries for each FNZ conformer was calculated at the same theoretical level described. All observed frequencies were positive (real numbers), verifying that they correspond to true minima on the potential energy surface of the system.

The results of the structural analysis of the FNZ conformers are shown in Table 2. They are similar to those reported by Chandrasekaran and Thilak Kumar,¹⁹ structurally optimized at the B3LYP/6-311++G(d,p) level and compared with X-ray diffraction analysis (XRD) crystallographic data.¹⁹

Shortening of the N–N bonds of the triazoles would indicate conjugation of the semicarbazoles. Also, the elongation of the C–N bonds would suggest intense electronic delocalization throughout the molecule.

The short interatomic distances between F33...H32 (2.269 Å), N27...H32 (2.142 Å), O31...H20 (2.558 Å), and O31...H15 (2.468 Å) for B3LYP and F33...H32 (2.243 Å), N27...H32 (2.137 Å), O31...H20 (2.506 Å), and O31...H15 (2.468 Å) for CAMB3LYP of FNZ conformer **I** indicate the possibility of intramolecular hydrogen bonding. Similarly, the short interatomic distances between F33...H13 (2.306 Å), F33...H16 (2.526 Å), N27...H32 (1.980 Å), O31...H15 (2.559 Å), and O31...H9 (2.359 Å) for B3LYP and F33...H13 (2.280 Å), F33...H16 (2.501 Å), N27...H32 (1.973 Å), O31...H15 (2.547 Å), and O31...H9 (2.692 Å) for CAMB3LYP of FNZ conformer **II** suggest intramolecular hydrogen bonding.

It can be seen from the dihedral angles C10–C5–C6–C1 and C10–C5–C4–C3 that the hydroxyl group attached to the difluorophenyl ring is slightly rotated, with the B3LYP method, 2.224° for conformer **I** and 3.138° for conformer **II**, and with the CAMB3LYP method, 2.217° for conformer **I** and 3.340° for conformer **II**, respectively. The methylene group attached to the triazole rings is even more rotated due to electronic conjugation, reflected in the dihedral angles C11–N22–N27–C24, C11–N22–C23–N28, C14–N17–N29–C19 and C14–N17–C18–N30. The triazole ring of FNZ conformer **II** that contains the N17–N20 bond showed a 180° rotation. These results are in line with those reported by the cited authors.¹⁹ Intramolecular charge transfer (ICT)

Table 2. Structural geometry parameters calculated for FNZ conformers **I** and **II**

Parameter	Bond length / Å				Parameter	Bond angle and dihedral angle / degree			
	B3LYP		CAM B3LYP			B3LYP		CAM B3LYP	
	I	II	I	II		I	II	I	II
C4–H9	1.084	1.084	1.083	1.083	C5–C10–O31	112.92	111.09	112.45	110.99
C10–O31	1.422	1.422	1.415	1.415	C14–C10–O31	103.93	105.31	104.15	105.39
O31–H32	0.977	0.977	0.975	0.979	C4–C5–C6	115.57	116.10	115.73	116.27
N22–N27	1.364	1.364	1.355	1.354	C5–C6–C1	123.80	124.09	123.90	124.08
N17–N29	1.365	1.365	1.356	1.355	C5–C4–C3	122.75	122.17	122.53	122.04
C24–N27	1.327	1.327	1.319	1.321	C3–C2–C1	122.04	122.29	122.13	122.37
C18–N17	1.355	1.355	1.348	1.347	H12–C11–H13	109.05	109.11	109.07	109.17
C11–N22	1.452	1.452	1.447	1.450	H15–C14–H16	108.23	109.26	108.22	109.33
C24–N28	1.361	1.361	1.356	1.353	C10–C5–C6–C1	179.08	178.44	179.06	178.35
C14–N17	1.453	1.453	1.448	1.446	C10–C5–C4–C3	–178.70	–178.43	–178.72	–178.32
C4–C5	1.407	1.407	1.400	1.395	C11–N22–N27–C24	–179.06	–179.38	–178.34	–178.87
C5–C6	1.402	1.402	1.395	1.391	C11–N22–C23–N28	179.18	179.54	178.36	178.95
C3–C4	1.395	1.395	1.390	1.391	C14–N17–N29–C19	178.29	–178.99	178.32	–178.28
C3–C2	1.388	1.388	1.383	1.383	C14–N17–C18–N30	–178.07	178.95	–178.10	178.14
C2–C1	1.387	1.387	1.382	1.384	C6–C5–C10–C14	149.97	–65.29	154.64	–65.58
C1–C6	1.391	1.391	1.384	1.381	C10–C5–C6–F33	–0.09	–1.50	–0.10	–1.58
C14–H16	1.091	1.091	1.090	1.090	C6–C5–C10–O31	32.37	177.57	37.00	177.44
C11–H13	1.094	1.090	1.093	1.090	C10–C14–N17–N29	121.91	123.27	105.30	104.97
					C10–C11–N22–N27	67.56	69.87	57.22	56.85
					C10–C14–N17–C18	–60.42	–59.00	–73.30	–72.61
					C10–C11–N22–C23	–111.22	–107.92	–122.00	–121.62
					C5–C10–C14–N17	–53.92	–54.40	–57.08	–56.51
					C5–C10–C11–N22	62.92	63.47	57.40	56.34

B3LYP: functional Becke, 3-parameter, Lee-Yang-Parr; CAM B3LYP: hybrid exchange correlation Coulomb Attenuated Method-Becke, 3-parameter, Lee-Yang-Parr.

from the electron-donor substituents to the phenyl ring could also be corroborated due to the shortening of the C–N bond distances, the lengthening of all C–C distances, and the contraction of the C4–C5–C6 internal angle. This is correlated with the increase of the two angles C5–C6–C1 and C5–C4–C3 in the union of the difluorophenyl ring and the triazole groups through the methylene group.

Dihedral angles C6–C5–C10–O31, C10–C14–N17–N29, C10–C11–N22–N27, C10–C14–N17–C18, C10–C11–N22–C23, C5–C10–C14–N17 and C5–C10–C11–N22 of FNZ molecules corresponding to seven conformers of four polymorphs crystallized by Karanam *et al.*²⁴ were compared. Similarly, the theoretical calculations of two new conformers were contrasted with their corresponding sets of torsion angles, obtained by the same research group.²⁴ None of our FNZ conformational structures fully agree in their torsion angles with those described in the literature.²⁴ However, all the torsion angles vary in a very small range (2–50°) which is equivalent to

differences of about 2 kcal mol^{–1}. This indicates that the FNZ has a high tendency to form numerous conformers in the gas phase. When these conformers crystallize in the form of crystal lattices, they can lead to the formation of different polymorphs by small changes in conformation.²⁴ Therefore, in theory, it would be possible to obtain crystalline polymorphs of conformations **I** and **II** of FNZ calculated as energetic minima.

Tables S1, S2, S3 and S4 (see Supplementary Information section) show the results of some molecular descriptors calculated based on the analysis of the frontier orbitals of the conformational structures **I** and **II** of FNZ, after being optimized with the bases B3LYP and CAMB3LYP. Data are ordered from vacuum to solvated states, by increasing solvent polarity, first nonpolar, then polar nonprotic, and finally polar protic. The effect of the various solvents on the FNZ molecule describes very well its energetic behavior, when passing from the gaseous phase to the solvent.

A small HOMO-LUMO gap means that the molecule is more reactive (soft molecule), while a large gap implies less molecular reactivity (hard molecule). Similarly, a small gap implies that the electron density of the molecule will change more easily than that of a hard molecule. In concordance with the previous parameters, the electrophilicity index is an indicator of energy reduction due to the electronic jump between the donor HOMO and the acceptor LUMO. On the other hand, electronegativity measures the power of attraction of electrons, classifying molecules as strong, moderate, or marginal.

Similarly, a high value of the electroaccepting power descriptor is indicative of a high capacity for electronic acceptance, while a low value of electrodonating power involves a better molecular system for electronic donation. Finally, the chemical potential is the amount of resistance to electron density loss.^{26,32} It has been reported that, with increasing solvent polarity, the total molecular energy of the solvated molecule should decrease and thus increase the stability of its molecular structure, which is evidenced by the rise in solute polarity.¹⁹

It is observed that the energy gap, hardness, and softness of FNZ **I** and **II** increase slightly as the polarity of the solvent increases, regardless of the optimization method used, which is indicative of the hardness of the API's structure. Therefore, FNZ has high chemical stability. However, the chemical potential decreases when the API goes through the gas phase to a solvated one. This is caused when the energetic transformation between the HOMO and the LUMO takes place. Considering FNZ's electronegativity, it varies slightly from vacuum to more polar solvents and its reduction is so small that it is not indicative of the ionization of covalent bonds in the solution, classifying the molecule as marginal.

Both the electroaccepting and the electrodonating power decline with solvation and when the polarity of the solvents rises. This reveals a certain drop in the electronic

acceptance capacity and an improvement in the tendency of the system to donate electrons in solution. Finally, the dipolar moment of the solute increases both, in the solvated phase and the increase of solvent polarity, presenting the highest maximum in DMSO and water, with important polarity within the selected non-protic and protic polar solvents, respectively. The evidence that FNZ has such a high dipolar moment in DMSO, a non-protic solvent, is indicative of the high polarizability inductive effect of the polar solvent affecting the API. These results are in agreement with the reference literature published by Chandrasekaran and Thilak Kumar.¹⁹

Experimental solvatochromic study

Table 3 shows the total number of solvents used, ordered according to their increasing polarity within their group: non-polar, polar aprotic and polar protic, indicating the physical constants of interest for our study and the empirical solvatochromic parameters of Kamlet and Taft, Catalán and Laurence equations.³⁹⁻⁴² The low solubility of FNZ in non-polar solvents prevents obtaining experimental data, therefore, they are used in the theoretical calculations of solvatochromism to have relevant information on the behavior of the API in non-polar solvents such as cyclohexane, with dipolar moment (μD) = 0 and parameters $\alpha = \beta = \pi^* = 0$, according to equation 1. The UV-Vis spectra of FNZ in solution are observed in Figure 3, with two absorption peaks at 261 and 266 nm.

Chandrasekaran and Thilak Kumar²¹ carried out an exhaustive theoretical study describing the effects of the solvent on FNZ. However, they only experimentally determined absorbance in three polar solvents: DMSO, methanol, and water. The authors relate the absorbance at $\lambda_{266\text{ nm}}$ due to $\pi-\pi^*$ transition and the one at $\lambda_{261\text{ nm}}$ to a $n-\pi^*$ transition. We disagree in this matter and state that both correspond to $\pi-\pi^*$ transitions. This is because both energy

Table 3. FNZ experimental values of wavelength, wavenumber and molar absorption coefficient

Solvent	Experimental					
	$\lambda_{261} / \text{nm}$	$\bar{\nu}_{261} / \text{cm}^{-1}$	$\epsilon_{261} / (\text{cm}^{-1} \text{M}^{-1})$	$\lambda_{266} / \text{nm}$	$\bar{\nu}_{266} / \text{cm}^{-1}$	$\epsilon_{266} / (\text{cm}^{-1} \text{M}^{-1})$
Diethyl ether	260.3	38.419	671.9	266.8	37.487	650.6
Dichloromethane	260.3	38.419	617.5	266.8	37.487	539.9
Acetonitrile	260.2	38.429	661.1	266.7	37.492	527.4
Dimethyl sulfoxide	261.0	38.313	569.1	267.4	37.392	536.0
2-Propanol	260.8	38.336	582.3	267.0	37.451	571.7
Ethanol	260.3	38.422	639.7	266.8	37.484	603.8
Methanol	260.3	38.422	659.6	266.5	37.523	637.2
Buffer pH 7.4	260.0	38.461	649.5	266.3	37.554	609.4

λ : wavelength; $\bar{\nu}$: wavenumber ($1/\lambda \cdot 10,000$); ϵ : molar absorption coefficient.

absorbances at 261 and 266 nm are very similar, as can be seen by the molar absorption coefficient in Table 3. This means that the nature of the electron jump is equivalent, and it is in the range of allowed or partially allowed electronic transitions, that correspond to π - π^* nature, as can be seen by $\log \epsilon_{266}$ ca. 2.8 and $\log \epsilon_{261}$ ca. 2.8. A n - π^* electronic transition is mostly forbidden in the UV-Vis range analyzed by symmetry selection rules, as a result of the different spatial regions of each orbital that leads to poor overlapping between them. Thus, this kind of electronic excitation appears at a higher wavelength and usually with little ϵ_{\max} , showed as a smaller absorption peak in the UV-Vis spectrum than a π - π^* .⁵⁰ The typical values of molar absorption coefficients (ϵ) for some electronic transitions in organic molecules are around: 10^4 - 10^5 $\text{cm}^{-1} \text{M}^{-1}$ for π - π^* in spin allowed of highly conjugated organic molecules, 200 - 500 $\text{cm}^{-1} \text{M}^{-1}$ for π - π^* in spin allowed with symmetry forbidden for small aromatic compounds, and 10 - 50 $\text{cm}^{-1} \text{M}^{-1}$ for spin allowed n - π^* for aromatic compounds with heteroatoms. Due to the high symmetry of FNZ, some π - π^* transitions may be symmetry forbidden and show significantly reduced molar absorption coefficients.⁵¹

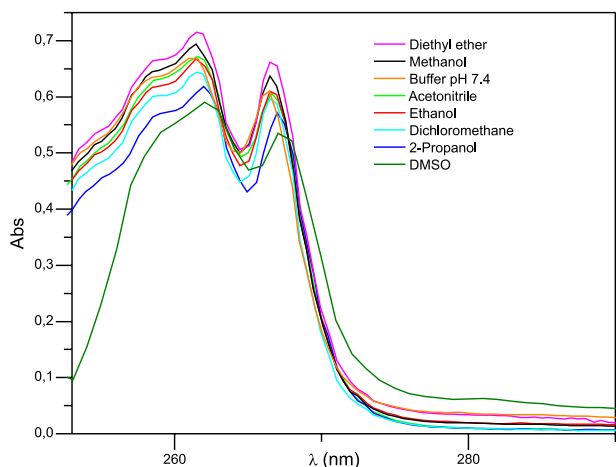


Figure 3. UV-Vis spectra of FNZ in different organic solvents.

According to the experimental data, a slightly bathochromic shift is observed as the polarity of the solvent increases. The change is greater when FNZ is surrounded by a polar solvent rather than non-polar one. It is caused by the polarization forces of attraction between the solvent and the API, which decreases the potential energy of the ground and excited states. This energy drop is higher for the excited state than for the ground state in π - π^* electron excitation. Therefore, the difference between the two levels decreases, resulting in a bathochromic shift.¹⁹

However, the solvent also affects the n - π^* electronic transitions, causing a hypsochromic shift due to unpaired

electron pairs. For this type of transition, the ground state is much more stable due to the effect of polar solvents on FNZ (hydrogen bonds forces). Consequently, the energies of the transition states are increased for polar solvents, with the subsequent hypsochromic shift of the spectrum.

In conclusion, a mixed effect results from the predominant interaction forces caused by a change in the solvent polarity and its ability to form hydrogen bonds. The signs and the relative contributions of the different coefficients of the solvation parameters in equations 1, 2, and 3, allow for discriminating opposite effects in the position of the molecular structure absorption maximum.⁴⁶

Considering the experimental solvatochromic shifts derived from the electronic transitions π - π^* illustrated in Table 3 and taking acetonitrile solvent ($\lambda_{\max} = 266.7$ nm) as a reference, we observe that when FNZ goes from aprotic solvents of lower polarity such as diethyl ether and dichloromethane to acetonitrile, hypsochromic shifts of 0.1 nm are produced in both cases, while towards DMSO the bathochromic shift is 0.7 nm.

From acetonitrile to protic polar solvents (2-propanol, ethanol, and methanol) the bathochromic shifts for the first and the second are 0.7 and 0.1 nm, respectively, while the hypsochromic shift for the third is 0.2 nm. Finally, when FNZ moves to the diprotic solvent water (in buffer pH 7.4 solution) a hypsochromic shift of 0.4 nm can be observed.

Solvents may be classified by different physical constants. Using viscosity (η) as a criterion, solvents are of low viscosity when their dynamic viscosity is < 2 mPa s at 20 °C, of medium viscosity between 2 and 10 mPa s, and of high viscosity above 10 mPa s.⁵²

Figure 4 shows a linear relationship between the maximum wavelength of FNZ and the viscosity of the solvents, where the λ_{\max} decreases as the η of the solvent

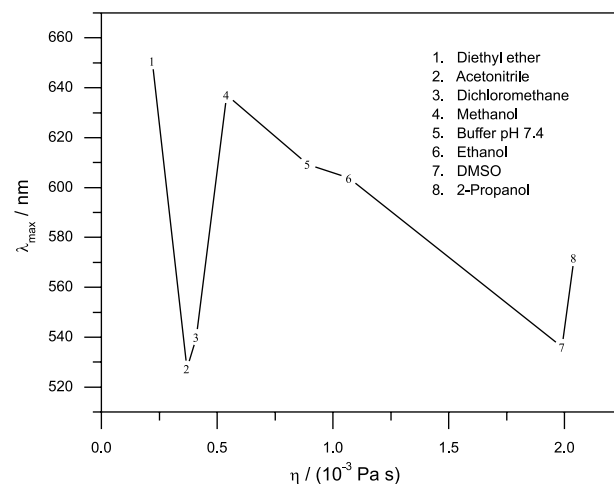


Figure 4. Maximum wavelength of FNZ in function of increasing solvent viscosity.

increases, although there are some exceptions as acetonitrile, dichloromethane, and 2-propanol. This data may indicate that the increasing viscosity of the solvent would be related to a hypsochromic behavior of the API, even though a mixed solvatochromism effect is caused by the change in the polarity of the solvent. Usually, no simple relationship with solvent viscosity was found when there has been an attempt to predict the solvent effect in the efficiency of a reaction due to an effective rate constant.⁵²

Table 4 shows the coefficients and errors associated with all the parameters of the multiple linear regressions in the FNZ solvatochromism analysis performed using the Kamlet and Taft, Catalán and Laurence equations. Also, the coefficient of determination, the relative contribution of each parameter, and the *p*-value of the Fisher statistic for the linear regression are reported. The results obtained both at $\lambda_{261\text{ nm}}$ and $\lambda_{266\text{ nm}}$ are quantitatively similar; however, all the parameters have statistical significance at 266 nm.

The triparametric equation 1 has a single parameter that accounts for the polarity-polarizability of the solvent, π^* , while the parameters α and β describe the acidity and basicity capacities of the solvent to donate or accept a proton via a hydrogen bond, respectively.

Our results explain 87% of the variability of $\bar{\nu}_{266}$ in different polar solvents. The greatest influence of the solvatochromism observed is due to the specific interactions, around 85% of the whole relative contributions. The β parameter accounts for around 50% of the total effect, while the α parameter explains the remaining 35% effect. Thus, the importance of the hydroxyl group attached to the methylene of FNZ, and the unpaired electron pairs of O and N can be deduced. The influence of non-specific interactions (given by the dihalogenated phenyl ring) is relatively low, although its influence on the global contribution to the solvatochromic effect is not neglected. The fact that the coefficients *s* and *b* have negative signs implies that the excited state is more stable as the polarity of the solvent increases, corresponding to a bathochromic shift. Contrariwise, the positive sign of the coefficient *a* shows the opposite influence.⁵³ Consequently, the net effect observed is a bathochromic behavior, given by the magnitude and sign of the most relevant coefficients, that is, the increase in the polarity of the polar solvents stabilizes the excited state of the electronic transitions of FNZ more than the basal state.

Equations 2 and 3 are tetraparametric, therefore, both have the advantage of differentiating the contributions of the non-specific interactions of the solvent on the

Table 4. Estimated coefficients and standard errors, correlations, significance, and the relative contributions percentage of the parameter's coefficients for multiple linear regression analysis of FNZ experimental data

Kamlet and Taft							
Wavelength / nm	A_0	<i>s</i>	<i>a</i>	<i>b</i>	R^2	<i>F</i>	
261	38,480.6 ± 48.6	-45.7 ± 51.3	76.2 ± 31.3	-158.2 ± 53.7	0.720	0.133	
		16%	27%	57%			
266	37,540.4 ± 31.4	-44.0 ± 33.2	95.5 ± 20.3	-138.1 ± 34.8	0.870	0.031	
		16%	34%	50%			
Catalán							
Wavelength / nm	A_0	c_{SP}	d_{sDP}	a_{SA}	b_{SB}	R^2	<i>F</i>
261	38,737.2 ± 98.2	-342.3 ± 150.7	-43.1 ± 60.3	11.6 ± 34.0	-152.5 ± 38.0	0.898	0.076
		62%	8%	2%	28%		
266	37,774.5 ± 48.6	-334.4 ± 74.5	-31.8 ± 29.8	46.5 ± 16.8	-113.5 ± 18.8	0.972	0.011
		65%	6%	8%	21%		
Laurence							
Wavelength / nm	A_0	<i>di</i>	<i>e</i>	a_1	b_1	R^2	<i>F</i>
261	38,776.9 ± 188.4	-427.3 ± 278.1	-30.7 ± 72.4	16.6 ± 37.6	-118.2 ± 51.9	0.840	0.144
		72%	5%	3%	20%		
266	37,780.2 ± 60.6	-346.9 ± 89.4	-39.7 ± 23.3	41.9 ± 12.1	-89.0 ± 16.7	0.982	0.006
		67%	8%	8%	17%		

R^2 : coefficient of determination; *F*: *p*-value of Fisher's statistic. A_0 : property of the solute to be correlated. Correlation coefficients of polarity-polarizability of the solvent (*s*), acidity (*a*) and basicity (*b*) of the solvent in Kamlet and Taft analysis. Correlation coefficients of solvent polarizability (c_{SP}), dipolarity (d_{sDP}), solvent acidity (a_{SA}), solvent basicity (b_{SB}) in Catalán analysis. Regression coefficients of dispersion and electronic induction interactions (*di*), electrostatic interactions (*e*), acidity (a_1) and basicity (b_1) of the solvent in Laurence analysis.

API in two different parameters, improving the previous analysis. The outcomes obtained from the analysis of the Catalán equation at 266 nm allow us to explain 97% of the variability of $\bar{\nu}_{266}$ in the solvation medium. It is remarkable that the coefficient of the parameter π^* of equation 1 was the least relevant of all, while in this case the magnitude of the parameter SP, the solvent polarizability, represents the largest relative contribution to the position of the maximum absorbance band. Regarding the order of magnitude, the basicity (SB), the acidity (SA), and the dipolarity (SdP) of the solvent, respectively showed statistical significance. The relative contribution of 65% of the $-c_{SP}$ coefficient, 21% of $-b_{SB}$ and 6% of $-d_{SdP}$ contribute to the bathochromic effect, contrasted to 8% of the a_{SA} coefficient, with a positive sign.

Similar findings were achieved with Laurence's equation 3. In this case, the parameter π^* is divided into two parameters, DI, representing the dispersion and electronic induction interactions, and ES, the electrostatic interactions between the permanent dipoles of the solute and the solvent.

The specific interactions are represented by α_1 and β_1 , the acidity and basicity of the solvent, respectively. The analysis yielded results like those obtained using the Catalán equation and allows us to explain 98% of the variability of $\bar{\nu}_{266}$ in the solvation medium, with a 67% relative contribution of the DI parameter. The contributions of solvent basicity (β_1), acidity (α_1) and permanent dipole interactions (ES), showed better statistical significance of the linear regression. Similarly, the magnitude and sign of the multiparameter coefficients determine a net bathochromic shift of the absorbance peak maximum, with a relative contribution of 67% from the coefficient $-di$, 17% from $-b_1$, 8% from $-e$ and 8% from a_1 .

Thus, non-specific interactions are evidenced as the most influential between the API and its solvation medium, given by polarizability and dispersion interactions and electronic induction of the FNZ dihalogenated phenyl ring and the solvent basicity (HBA capacity) given by the hydroxyl group of the molecule. The solvatochromic analysis confirms that when the polarity of the solvent increases, the excited state stabilizes more than the basal state of FNZ, being the first one of higher polarity and lower energy, typical of the bathochromism observed.^{13,27,41,44,52}

The International Union of Pure and Applied Chemistry (IUPAC) has defined the concept of pharmacophore or pharmacophore pattern as "the ensemble of steric and electronic features that is necessary to ensure the optimal supramolecular interactions with a specific biological target structure and to trigger (or to block) its biological response".⁵⁴ A pharmacophore does not represent a real molecule or a real association of functional groups, but rather a purely abstract concept that accounts for the common molecular

interaction capacities of a group of compounds towards their target structure. The pharmacophore can be considered as the largest common denominator shared by a set of active molecules. This definition discards a common misuse in medicinal chemistry that consists of naming as simple chemical functionalities such as guanidines, sulfonamides or dihydroimidazoles (formerly imidazolines), or typical structural skeletons such as flavones, phenothiazines, prostaglandins or steroids as pharmacophores.⁵⁵ Ji *et al.*⁵⁶ have studied the pharmacophoric conformations of 14 azole antifungals, which have a similar docking mode at the active site of the enzyme lanosterol 14- α -demethylase from *Candida albicans*.

The halogenated phenyl group of azole inhibitors is deep in the same hydrophobic binding cleft as the 17-alkyl chain of the substrate. Interactions of π - π stacking could exist between the halogenated phenyl ring and the aromatic ring of residue Y132 in the hydrophobic cavity of the active site, which increases the fungicidal activity of the API.⁵⁶ This information is consistent with the large relative contribution of the SP and DI parameters of the Catalán and Laurence equations and is in agreement with the experimental bathochromic behavior of FNZ in solution.

It has also been suggested that the oxygen atom attached to C10 is favorable to antifungal activity for two reasons. First, the chirality of that carbon atom gives it greater antifungal activity than other stereoisomers, for which FNZ led a new generation of more powerful, better tolerated, and metabolically more stable antifungals. Second, the oxygen atom interacts with the water molecules conserved in the active site forming hydrogen bonds to bind it to the H310 residue of the protein.⁵⁶

Recently, crystallographic data of the lanosterol 14- α -demethylase-fluconazole complex from *Saccharomyces cerevisiae* provided information on a water-mediated hydrogen bond network between the API and the enzyme. Two water molecules form networks of hydrogen bonds with FNZ. The first water molecule mediates the hydrogen bonds between the hydroxyl groups of FNZ and Y140, as well as a propionate of the heme cofactor. The second forms hydrogen bonds with the carbonyl oxygen of S382, the hydroxyl of Y126, and the atom N4' of the second triazole ring furthest from heme.⁵⁷ The previous evidence agrees with the relative contribution of the SB and β_1 parameters of the Catalán and Laurence equations, with the same bathochromic effect on the solvation of FNZ. On the other hand, the relative contribution of the SA and α_1 parameters of the Catalán and Laurence equations in the inhibition function of the N4' in the second triazole ring is evident, thus indicating the HBD solvent capacity, although small and hypsochromic.

Theoretical solvatochromic study

Table 5 summarizes the spectral behavior of both optimized conformers of FNZ in all the solvents studied. They are ordered by increasing polarity. The shifts of the absorption band in the UV-Vis in each solvent are similar to the experimental and theoretical data reported in the literature.¹⁹ All the theoretical λ in the UV-Vis region are lower than the experimental ones. The λ obtained with conformer **II** are lower than those of conformer **I**, and the λ obtained by CAMB3LYP are lower than those calculated by B3LYP. Every one of the values achieved corresponds to π - π^* transitions, due to HOMO-LUMO electronic excitations. Taking the solvent acetonitrile as a reference, we observe that FNZ conformer **I** ($\lambda_{\text{B3LYP}} = 235.7$ nm) shows on average hypsochromic shifts of 0.7 nm from non-polar solvents such as cyclohexane, tetrachloromethane, and benzene. When FNZ moves from aprotic solvents of lower polarity, such as diethyl ether and dichloromethane to acetonitrile, hypsochromic shifts of 0.3 and 0.2 nm are produced, respectively, while towards DMSO no shift was observed. Similarly, a bathochromic shift of 0.1 nm is obtained when moving to the protic polar solvent ethanol, while there is no change for the protic solvents methanol or water. Similar behaviors are displayed in all the theoretical calculations described.

Tables 6 and 7 show the coefficients and errors associated with the parameters of the solvatochromism analysis of both FNZ conformers calculated by equations 1, 2, and 3. Also, the coefficient of determination, the relative contribution of each parameter, and the p -value of the Fisher statistic for the linear regression are reported. At

first, the analysis is performed only by including polar solvents to compare them with the experimental results already obtained. Next, non-polar solvents data are included to consider the zero or nearly zero contributions of their solvatochromic parameters.

With respect to the theoretical solvatochromic analysis obtained by both the B3LYP and CAMB3LYP methods and evaluated by Kamlet and Taft with $n = 7$, it is observed that only the parameters π^* and α are significant, with a similar percentage for both conformers. However, considering $n = 10$ for both methods, the significant parameters are π^* and β , with a relative contribution of 44% for s and 42% for b , with 78% of the variability for conformer **I** by CAMB3LYP, displaying greater statistical significance. All coefficients have a positive sign, corresponding to a hypsochromic shift.

The theoretical multiparametric analysis of Catalán with $n = 7$ by the B3LYP method showed significance in all parameters in both conformers, with similar results. The relative contribution of the parameters corresponding to non-specific interactions changed drastically with respect to the experimental analysis, being almost the same in the theoretical study: 50% of d_{sdP} and 39% of $-c_{\text{SP}}$. The relative contribution of specific interactions is similar, around 6% in both a_{SA} and b_{SB} . By raising the number of solvents to $n = 10$, the SA contribution loses significance, increasing the statistical significance of the whole linear regression by two orders of magnitude. With the CAMB3LYP method, the results are like those obtained for both conformers, reducing the representativeness of the specific interactions in conformer **II** with $n = 10$ and minimizing the acid character of the solvent in conformer **I**. Although this

Table 5. FNZ theoretical values of wavelength and wavenumber with f at the TD-DFT/6-31+G(d) level of theory

Solvent	Conformer I						Conformer II					
	B3LYP			CAMB3LYP			B3LYP			CAMB3LYP		
	$\lambda_{\text{max}} / \text{nm}$	$\bar{\nu}_{\text{max}} / \text{cm}^{-1}$	f	$\lambda_{\text{max}} / \text{nm}$	$\bar{\nu}_{\text{max}} / \text{cm}^{-1}$	f	$\lambda_{\text{max}} / \text{nm}$	$\bar{\nu}_{\text{max}} / \text{cm}^{-1}$	f	$\lambda_{\text{max}} / \text{nm}$	$\bar{\nu}_{\text{max}} / \text{cm}^{-1}$	f
Cy	236.4	42.301	0.021	228.2	43.829	0.021	234.8	42.588	0.014	226.9	44.084	0.013
Tet	236.4	42.310	0.021	228.1	43.835	0.021	234.8	42.591	0.014	226.8	44.086	0.013
Ben	236.4	42.308	0.022	228.1	43.833	0.022	234.8	42.590	0.014	226.9	44.082	0.013
DE	236.0	42.373	0.017	227.9	43.889	0.019	234.6	42.628	0.013	226.7	44.115	0.012
DCM	235.9	42.394	0.019	227.8	43.904	0.019	234.6	42.637	0.013	226.7	44.119	0.013
AcN	235.7	42.423	0.018	227.6	43.931	0.018	234.5	42.651	0.012	226.6	44.133	0.012
DMSO	235.7	42.416	0.018	227.7	43.923	0.018	234.5	42.646	0.013	226.6	44.127	0.012
EtOH	235.6	42.418	0.018	227.7	43.927	0.018	234.5	42.650	0.012	226.6	44.129	0.012
MeOH	235.7	42.423	0.017	227.6	43.933	0.017	234.5	42.653	0.012	226.6	44.133	0.012
Water	235.7	42.427	0.017	227.6	43.935	0.017	234.4	42.55	0.012	226.6	44.135	0.012

Cy: cyclohexane; Tet: tetrachloromethane; Ben: benzene; DE: diethyl ether; DCM: dichloromethane; AcN: acetonitrile; DMSO: dimethyl sulfoxide; EtOH: ethanol; MeOH: methanol; B3LYP: functional Becke, 3-parameter, Lee-Yang-Parr; CAM B3LYP: hybrid exchange correlation Coulomb Attenuated Method-Becke, 3-parameter, Lee-Yang-Parr; λ : wavelength; $\bar{\nu}$: wavenumber ($1/\lambda \cdot 10,000$); f : oscillator strength.

Table 6. Estimated coefficients and standard errors, correlations, significance, and the relative contributions percentage of the parameter's coefficients for multiple linear regression analysis of FNZ conformer **I** theoretical data

Kamlet and Taft	A_0	s	a	b	R^{2c}	F^t	
	$42,366.9 \pm 20.8^c$	38.8 ± 22.8	17.3 ± 13.5	16.5 ± 24.3	0.709	0.242	
B3LYP ^a		53%	24%	23%			
	$42,303.1 \pm 20.3^d$	77.1 ± 33.3	20.8 ± 26.6	69.9 ± 41.0	0.782	0.021	
		46%	12%	42%			
CAMB3LYP ^b		30.4 ± 19.9	17.00 ± 11.8	15.1 ± 21.2	0.712	0.238	
		49%	27%	24%			
	$43,883.3 \pm 18.2^c$	62.3 ± 28.2	20.1 ± 22.5	60.0 ± 34.8	0.783	0.021	
		44%	14%	42%			
Catalán	A_0	c_{SP}	d_{SDP}	a_{SA}	b_{SB}	R^2	F^t
	$42,375.6 \pm 15.7^c$	-72.0 ± 24.4	92.0 ± 9.8	7.4 ± 5.5	13.0 ± 7.2	0.987	0.026
B3LYP		39%	50%	4%	7%		
	$42,381.0 \pm 42.7^d$	-111.1 ± 57.4	112.5 ± 14.1	5.7 ± 15.4	21.4 ± 19.5	0.973	0.0004
		44%	45%	2%	9%		
CAMB3LYP		-74.9 ± 18.6	79.3 ± 7.4	8.1 ± 4.2	13.2 ± 5.5	0.99	0.020
		43%	45%	5%	7%		
	$43,897.4 \pm 12.0^c$	-104.4 ± 46.5	93.4 ± 11.4	7.0 ± 12.5	19.1 ± 15.8	0.976	0.0003
		47%	42%	3%	8%		
Laurence	A_0	di	e	a_1	b_1	R^2	F^t
	$42,427.5 \pm 12.0^c$	-106.0 ± 17.6	82.5 ± 4.6	-1.6 ± 2.4	-6.0 ± 3.5	0.997	0.006
B3LYP		54%	42%	1%	3%		
	$42,500.2 \pm 48.5^d$	-247.0 ± 60.6	124.4 ± 14.7	-17.0 ± 10.1	-1.6 ± 18.0	0.979	0.0002
		63%	32%	4%	1%		
CAMB3LYP		-105.8 ± 14.6	70.3 ± 3.8	-1.0 ± 2.0	-2.3 ± 2.9	0.997	0.006
		59%	39%	1%	1%		
	$44,001.4 \pm 37.0^d$	-215.7 ± 46.3	102.2 ± 11.6	-12.9 ± 7.7	0.8 ± 13.7	0.983	0.0001
		65%	31%	4%	0%		

^aB3LYP: functional Becke, 3-parameter, Lee-Yang-Parr; ^bCAM B3LYP: hybrid exchange correlation Coulomb Attenuated Method - Becke, 3-parameter, Lee-Yang-Parr; ^cn = 7; ^dn = 10; ^ecoefficient of determination; ^fp-value of Fisher's statistic. A_0 : property of the solute to be correlated. Correlation coefficients of polarity-polarizability of the solvent (s), acidity (a) and basicity (b) of the solvent in Kamlet and Taft analysis. Correlation coefficients of solvent polarizability (c_{SP}), dipolarity (d_{SDP}), solvent acidity (a_{SA}), solvent basicity (b_{SB}) in Catalán analysis. Regression coefficients of dispersion and electronic induction interactions (di), electrostatic interactions (e), acidity (a_1) and basicity (b_1) of the solvent in Laurence analysis.

method better explains the variability of $\bar{\nu}$ in the solvation environment, with 98%, the highest statistical significance is obtained with the B3LYP method.

Finally, the theoretical analysis of the results obtained with the B3LYP method and carried out by applying the Laurence equation with n = 7 resulted in more than 99% of the variability for both conformers. The relative contribution of the non-specific interactions varied slightly, compared with Catalán equation. The electronic dispersion and induction were above the interactions between the permanent dipoles of the API and the solvent. As regards specific interactions, the solvent acidity was almost irrelevant.

With n = 10, the difference between the proportion of DI and ES interactions increased, where -di is greater than 60% and e is around 30%, without relevance of the

basicity of the solvent and a greater statistical significance in the linear regression analysis. Using the CAMB3LYP method, similar results were obtained as with B3LYP, with a representativeness of more than 99% of the response variable for both conformers in the case of n = 7, and the highest statistical significance with n = 10. In the latter case, both conformers have a high relative contribution of the DI and ES parameters, as well as the ability to accept hydrogen bonds, α_1 , and without relevance of the capacity to give hydrogen bonds, β_1 . The net spectroscopic shift is bathochromic due to the magnitudes and signs of the coefficients: -di, e, $-a_1$, and b_1 . It should be noted that although ES has a smaller magnitude than DI with respect to the type of interaction it represents, its statistical error is much lower, and its influence on the API solvation is more reliable.

Table 7. Estimated coefficients and standard errors, correlations, significance, and the relative contributions percentage of the parameter's coefficients for multiple linear regression analysis of FNZ conformer **II** theoretical data

Kamlet and Taft	A_0		s	a	b	R^{2c}	F^T
	$42,625.5 \pm 9.9^c$		16.4 ± 10.8	11.1 ± 6.4	6.5 ± 11.5	0.740	0.207
B3LYP ^a			48%	33%	19%		
	$42,588.9 \pm 11.2^d$		38.6 ± 18.4	13.0 ± 14.7	36.9 ± 22.7	0.766	0.025
			44%	15%	41%		
	$44,112.8 \pm 8.0^c$		11.4 ± 8.7	8.2 ± 5.2	4.8 ± 9.3	0.696	0.257
CAMB3LYP ^b			47%	34%	19%		
	$44,084.3 \pm 9.1^d$		28.1 ± 15.0	10.0 ± 12.0	28.8 ± 18.3	0.740	0.034
			42%	15%	43%		
Catalán	A_0	c_{SP}	d_{SDP}	a_{SA}	b_{SB}	R^2	F
	$42,635.9 \pm 7.0^c$	-44.8 ± 10.7	43.4 ± 4.3	5.7 ± 2.4	5.7 ± 3.1	0.990	0.020
B3LYP		45%	44%	6%	5%		
	$42,639.1 \pm 24.3^d$	-72.0 ± 32.8	58.5 ± 8.0	4.1 ± 8.8	11.4 ± 11.1	0.970	0.0005
		49%	40%	3%	8%		
	$44,125.8 \pm 5.8^c$	-41.4 ± 9.1	32.7 ± 3.6	3.4 ± 2.0	3.0 ± 2.7	0.987	0.026
CAMB3LYP		51%	41%	4%	4%		
	$44,130.3 \pm 21.1^d$	-65.9 ± 28.4	44.8 ± 7.0	2.0 ± 7.6	7.5 ± 9.6	0.961	0.001
		55%	37%	2%	6%		
Laurence	A_0	di	e	a_1	b_1	R^2	F
	$42,660.6 \pm 5.8^c$	-60.4 ± 8.5	38.1 ± 2.2	0.7 ± 1.1	-2.7 ± 1.7	0.997	0.006
B3LYP		59%	37%	1%	3%		
	$42,704.4 \pm 28.8^d$	-145.3 ± 36.0	63.3 ± 8.8	-8.7 ± 6.0	-0.1 ± 10.7	0.974	0.0004
		67%	29%	4%	0%		
	$44,148.3 \pm 5.2^c$	-59.4 ± 7.7	28.9 ± 2.0	-0.7 ± 1.0	-1.1 ± 1.5	0.996	0.009
CAMB3LYP		66%	32%	1%	1%		
	$44,183.6 \pm 21.5^d$	-125.3 ± 27.0	47.2 ± 6.5	-7.8 ± 4.5	0.3 ± 8.0	0.975	0.0003
		69%	26%	4%	1%		

^aB3LYP: functional Becke, 3-parameter, Lee-Yang-Parr; ^bCAM B3LYP: hybrid exchange correlation Coulomb Attenuated Method - Becke, 3-parameter, Lee-Yang-Parr; ^cn = 7; ^dn = 10; ^ecoefficient of determination; ^fp-value of Fisher's statistic. A_0 : property of the solute to be correlated. Correlation coefficients of polarity-polarizability of the solvent (s), acidity (a) and basicity (b) of the solvent in Kamlet and Taft analysis. Correlation coefficients of solvent polarizability (c_{SP}), dipolarity (d_{SDP}), solvent acidity (a_{SA}), solvent basicity (b_{SB}) in Catalán analysis. Regression coefficients of dispersion and electronic induction interactions (di), electrostatic interactions (e), acidity (a_1) and basicity (b_1) of the solvent in Laurence analysis.

In short, the interactions of electronic polarizability, dispersion, and induction are equally important in theoretical and experimental solvatochromic behavior, and according to which equation is analyzed, Catalán or Laurence, and which method, B3LYP or CAMB3LYP, it takes on a certain relevance the acidity or basicity of the solvent. Both, B3LYP and CAMB3LYP methods, present the same percentage of explanation of the dependent variable with similar statistical significance. However, the theoretical results obtained with the B3LYP method are closer to the experimental values of λ_{max} than with the CAMB3LYP method.

Figures S1 and S2 (see Supplementary Information section) show theoretical wavelength values for both FNZ conformers. The main difference between the two structures

is that π - π^* electronic transitions in polar solvent for FNZ conformer **II** are stronger than the ones in conformer **I** for the similar kind of solvents. The theoretical and experimental UV-Vis spectra were not depicted together in a single figure due to the differences in wavelength between the obtained data with the basis sets used for the analysis.

Thermochromic study

Figure 5 reveals the variation of the absorbance spectrum of FNZ in buffer solution at pH 7.4 due to the temperature gradient to which the solution was exposed. The thermal gradient plotted increases each line in 20 °C from 5 to 65 °C, although the measurements were performed every 5 °C. The analysis of the thermochromic study

makes evident the existence of three clearly identifiable isosbestic points at 262.4, 265.0, and 267.6 nm, without crossing the spectra in other positions. This correlates with intermolecular equilibria of the FNZ in the buffer, but not with intramolecular equilibria.

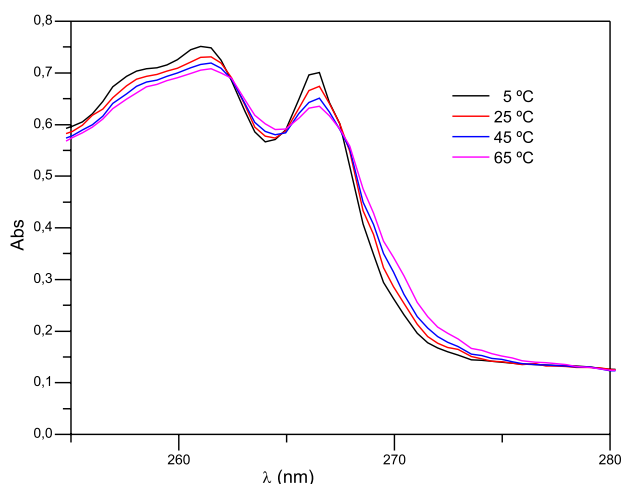


Figure 5. Thermochromism of FNZ in buffer pH 7.4.

Three acid-base constants have been described for FNZ, according to its ability to give up H^+ , given by the $-OH$ group of C10 or to accept H^+ , by any of the $-N$ of the triazole groups 1,2,4-triazole.⁴⁹ They are congruent with the three isosbestic points found in the API thermochromic study, where three intermolecular acid-base equilibria are proposed: $pK_a HA = 11.93$, $pK_{ab1} BH^+ = 5.23$ and $pK_{ab2} BH_2^+ = 1.76$ (Figure 6).

The stability of the molecule and charge delocalization of FNZ were studied by Chandrasekaran and Thilak Kumar,¹⁹ who analyzed the number of electrons or natural population, the natural bonding orbitals, and the natural local molecular orbitals by molecular modeling calculations with the B3LYP/6-311++G(d,p) method. These results showed that the charge of the lone pairs of the $N4'$ of each 1,2,4-triazole group is slightly higher than that of the other nitrogen atoms in the molecule. The $N4'$ atom becomes more electronegative, since the quantity of charges transferred from the $n(N4')$ orbital is very low, which makes the triazole ring a highly chelating agent, susceptible to protonation or hydrogen bonding. Therefore, the acid-base equilibria that are related to the isosbestic points probably would correspond to the loss of H^+ from the C10 hydroxyl group, and to the gain of one H^+ in each of the $N4'$ of the azole rings, as illustrated in Figure 6 (boxed intermolecular equilibria).

The importance of the $N4'$ of the azole ring as a chelating agent is highlighted by considering it as part of the azole pharmacophore, rather than $N1'$ or $N2'$, since the

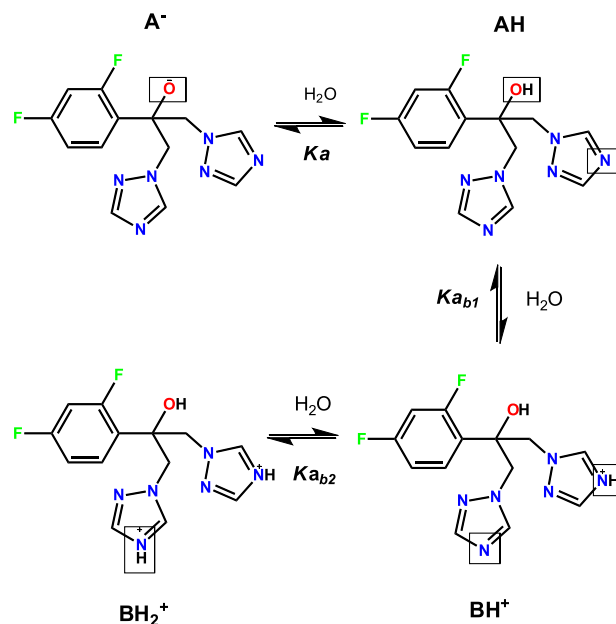


Figure 6. The acid-base equilibria of the antifungal FNZ.

$N4'$ of the azole ring is covalently bound to the heme of the target substrate. The compound would be deprived of activity if $N4'$ is replaced by a carbon atom.¹⁹ More recent crystallographic studies of the binding of the enzyme to FNZ confirm the importance of the $N4'$ of the triazoles by demonstrating coordination bonding of the nitrogen atom $N4'$ in the triazole ring with the heme iron, replacing the water ligand and stabilizing the low spin bond. The triazole ring of FNZ coordinates with iron within the heme cofactor ($Fe \cdots N$ distance 2.13 Å), corroborated by spectrophotometric data.⁵⁵ As already mentioned, the $N4'$ of the other triazole participates in the network of hydrogen bonds with the residues of the active site outside the heme group.

Conclusions

The theoretical study of FNZ using the bases DFT-B3LYP/6-31+G(d) and DFT-CAMB3LYP/6-31+G(d) allows the geometric optimization of two structural conformers of the API corresponding to two true minima of energy potential. Both conformers show high electronic delocalization in the semicarbazoles, intramolecular charge transfer from the electron-donor substituents to the phenyl ring, the possibility of forming numerous intramolecular hydrogen bonds, and the same probability of crystallizing in different polymorphs when forming crystal lattices. The analysis of the molecular descriptors allows us to appreciate that both structures present great chemical stability and can be classified as marginal according to their electronegativity. Their dipolar moments rise in the solvated

phase as the polarity of the solvent increases, which indicates the high inductive effect of the polarizability of the polar solvent that affects the FNZ molecule.

The experimental solvatochromic study of FNZ results in a slightly bathochromic shift as the solvent polarity increases, given by π - π^* electronic transitions. The multiparametric equations of Catalán and Laurence were more efficient than Kamlet and Taft's equation. The magnitudes and signs of the coefficients of the solvatochromic parameters of Catalán and Laurence agree in their relative relevance, around 65% of the SP parameter, solvent polarizability, and DI, electronic dispersion and induction, both related to π - π stacking type interactions between the dihalogenated phenyl ring of FNZ and the aromatic ring of residue Y132 in the hydrophobic cavity of the active site. Similarly, with a negative sign and a relative relevance of 20%, the parameters SB and β_1 become important, both indicative of the solvent basicity (HBA ability), consistent with the network of hydrogen bonds mediated by water between the API and the enzyme, specifically the hydroxyl group of FNZ and the Y140 residue. To a lesser extent, and with a positive sign, 8% of the SA and α_1 parameters are observed, related to the solvent acidity (HBD capacity). Even though it is a low value, it shows the importance of the N4' in the furthest triazole beyond the heme group within the water-mediated hydrogen bonding network.

The theoretical study of the solvatochromism of FNZ includes non-polar solvents in the multiparameter equations and confirms the bathochromic shift of the maximum of the spectral line as the polarity of the solvent increases. However, the relative relevance of the solvatochromic parameters changes. On average, 90% of the relevant interactions correspond to non-specific interactions, with polarizability/dispersion and electronic induction prevailing over dipolarity/interaction of permanent dipoles between solute and solvent. As the predominant interaction forces have opposite signs, a mixed solvatochromic resulting effect is observed, combined with the negative coefficients of the specific interaction parameters. Regarding the TD-DFT methods used, both B3LYP and CAMB3LYP result in shorter wavelengths than experimentally, matching the available bibliography. In our case, the theoretical results obtained with the B3LYP method are closer to the experimental values of λ_{\max} than with the CAMB3LYP method.

The thermochromic study shows intermolecular acid-base balances consistent with the three pK_a of the FNZ, showing the deprotonation of the R-OH group and the protonation of each of the N4' of theazole rings, the most electronegative of each triazole. Similarly, the importance of N4' is evident by the coordination bond of the N4' atom

in the triazole ring with heme iron, which is essential for the manifestation of antifungal activity. Both nonspecific interactions and hydrogen bonding of FNZ correlate with substrate binding and antifungal activity, which is inherent to the proposed pharmacophore for azoles. The suggested ionization equilibria at physiological pH justify a very good oral and intravenous bioavailability and effective tissue distribution of the API.

Besides the former pharmacological action fully analyzed against several kinds of fungi, the physicochemical properties of FNZ studied in this research work complement the available scientific data. In the future, this information could lead to reposit this drug as an API for new therapeutic targets.

Supplementary Information

Supplementary information shows the results of some molecular descriptors calculated based on the analysis of the frontier orbitals of the conformational structures **I** and **II** of FNZ, after being optimized with the bases B3LYP and CAMB3LYP. Also, there were depicted the theoretical wavelength of both FNZ conformers, to compare their interaction with different organic solvents.

Supplementary information (Tables S1, S2, S3, S4 and Figures S1-S4) is available free of charge at <http://jbc.sbp.org.br> as PDF file.

Acknowledgments

This work was supported by Instituto de Tecnología Aplicada de la Universidad Nacional de la Patagonia Austral (grant No. PI 29/A436-1-ITA and PI 29/A486-1-ITA) and Grupo de Química Medicinal del Centro Regional de Investigación y Desarrollo Científico Tecnológico de la Facultad de Ciencias Naturales y Ciencias de la Salud de la Universidad Nacional de la Patagonia San Juan Bosco (grant No. PI 1490 Código SIGEVA-80020180200020UP and PI 1712 Código SIGEVA- 80020210100006UP).

We would like to thank LaIC, the Scientific English Laboratory of the UNPA, for reviewing the English manuscript.

Author Contributions

All authors contributed to the study, conception, and design. Conceptualization of the research was made by Fernando Gabriel Olivares, Juan Pablo Escalada and Graciela Pinto Vitorino. Quality control and preparation of experimental samples (resources) were performed by Francisco Gabriel Lazcano, Fernando Gabriel Olivares and María Gloria Barúa. Solvatochromic experimental data collection, data curation and formal analysis were accomplished by Fernando

Gabriel Olivares, María Gloria Barúa, Juan Pablo Escalada and Graciela Pinto Vitorino. Theoretical calculation data collection, data curation and formal analysis were done by Fernando Gabriel Olivares, Marcelo Omar Castillo, and Graciela Pinto Vitorino. Thermochemical techniques were performed by Fernando Gabriel Olivares and María Gloria Barúa. The UV-Vis spectrum was interpreted by Fernando Gabriel Olivares, María Gloria Barúa, Juan Pablo Escalada and Graciela Pinto Vitorino. The validation of the data obtained, and the funding acquisitions were achieved by Fernando Gabriel Olivares, Juan Pablo Escalada and Graciela Pinto Vitorino. The first draft of the manuscript was written by Fernando Gabriel Olivares and all authors commented on previous versions of the manuscript. All authors read and approved the final manuscript.

References

1. Campoy, S.; Adrio, J. L.; *Biochem. Pharmacol.* **2016**, *133*, 86. [Crossref]
2. Garcia-Rubio, R.; Monteiro, M. C.; Mellado, E. In *Encyclopedia Mycology*, vol. 1; Zaragoza, O.; Casadevall, A., eds.; Elsevier: Netherlands, 2021, p. 427. [Crossref]
3. Espinel-Ingroff, A. In *Reference Module in Biomedical Sciences Schmidt*, T. M., ed.; Elsevier: Netherlands, 2019, p. 140. [Crossref]
4. Shafiei, M.; Peyton, L.; Hashemzadeh, M.; Foroumadi, A.; *Bioorg. Chem.* **2020**, *104*, 104240. [Crossref]
5. Allen, D.; Wilson, D.; Drew, R.; Perfect, J.; *Expert Rev. Anti-Infect. Ther.* **2015**, *13*, 787. [Crossref]
6. Nett, J. E.; Andes, D. R.; *Infect. Dis.* **2016**, *30*, 51. [Crossref]
7. Jourdan, J. P.; Bureau, R.; Rochais, C.; Dallemagne, P.; *J. Pharm. Pharmacol.* **2020**, *72*, 1145. [Crossref]
8. Ashburn, T. T.; Thor, K. B.; *Nat. Rev. Drug Discovery* **2004**, *3*, 673. [Crossref]
9. Novac, N.; *Trends Pharmacol. Sci.* **2013**, *34*, 267. [Crossref]
10. da Silva, W. V.; da Silva, W. V.; Holanda, V. N.; *Interfaces* **2020**, *8*, 636. [Crossref]
11. Lemke, T. L.; Roche, V. F.; Zito, S. W.; *Review of Organic Functional Groups: Introduction to Medicinal Organic Chemistry*; Wolters Kluwer Health/Lippincott Williams & Wilkins: New York, 2012, ch. 1.
12. Almandoz, M. C.; Sancho, M. I.; Duchowicz, P. R.; Blanco, S. E.; *Spectrochim. Acta, Part A* **2014**, *129*, 52. [Crossref]
13. Miotke, M. M.; Józefowicz, M.; *J. Mol. Liq.* **2017**, *230*, 129. [Crossref]
14. Kosenkov, D.; Slipchenko, L.; *J. Phys. Chem. A* **2011**, *115*, 392. [Crossref]
15. Suppan, P.; Ghoneim, N.; *Solvatochromism*; Royal Society of Chemistry: England, 1997, ch. 2.
16. Mancini, P. M.; Adam, C.; Pérez, A. C.; Vottero, L. R.; *J. Phys. Org. Chem.* **2000**, *13*, 221. [Crossref]
17. Marcus, Y.; *The Properties of Solvents*, Wiley Series in Solution Chemistry, vol. 4; John Wiley & Sons Ltd: England, 1998, ch. 2.
18. Marcus, Y.; *Solvent Mixtures: Properties and Selective Solvation*; CRC Press: New York, 2002, ch. 1.
19. Chandrasekaran, K.; Thilak Kumar, R.; *Spectrochim. Acta, Part A* **2015**, *150*, 974. [Crossref]
20. Day, J. H.; *Chem. Rev.* **1963**, *63*, 65. [Crossref]
21. Ghasemi, J.; Niazi, A.; Westman, G.; Kubista, M.; *Talanta* **2004**, *62*, 835. [Crossref]
22. Santo, M.; Giacomelli, L.; Cattana, R.; Silber, J.; Blanco, M. M.; Schapira, C. B.; Perillo, I. A.; *Spectrochim. Acta, Part A* **2003**, *59*, 1399. [Crossref]
23. Bhesaniya, K.; Nandha, K.; Baluja, S.; *J. Chem. Eng. Data* **2014**, *59*, 649. [Crossref]
24. Karanam, M.; Dev, S.; Choudhury, A. R.; *Cryst. Growth Des.* **2011**, *12*, 240. [Crossref]
25. Lee, C.; Yang, W.; Parr, R. G.; *Phys. Rev. B* **1988**, *37*, 785. [Crossref]
26. Al-Wahaibi, L. H.; Abdalla, M.; Sheena M. Y.; Shyma M. Y.; Costa, R. A.; Rana, M.; El-Emam, A. A.; Hassan, H. M.; Al-Shaalan, N. H.; *Polycyclic Aromat. Compd.* **2022**. [Crossref]
27. Airinei, A.; Isac, D. L.; Homocianu, M.; Cojocaru, C.; Hulubei, C.; *J. Mol. Liq.* **2017**, *240*, 476. [Crossref]
28. Yanai, T.; Tew, D. P.; Handy, N. C.; *Chem. Phys. Lett.* **2004**, *393*, 51. [Crossref]
29. Kujawski, J.; Czaja, K.; Dettlaff, K.; Żwawiak, J.; Ratajczak, T.; Bernard, M. K.; *J. Mol. Struct.* **2019**, *1181*, 179. [Crossref]
30. Kujawski, J.; Czaja, K.; Jodłowska-Siewert, E.; Dettlaff, K.; Żwawiak, J.; Kujawski, R.; Ratajczak, T.; Bernard, M. K.; *J. Mol. Struct.* **2017**, *1146*, 259. [Crossref]
31. Skyner, R. E.; McDonagh, J. L.; Groom, C. R.; van Mourik, T.; Mitchell, J. B. O.; *Phys. Chem. Chem. Phys.* **2015**, *17*, 6174. [Crossref]
32. Choque Aspiazú, R.; Nogales, J.; Apaza Torrez, N.; *Rev. Cs. Farm. Bioq.* **2020**, *8*, 37. [Crossref]
33. Figueredo, S. F.; Páez, M. S.; Torres, F.; *Quim. Nova* **2017**, *40*, 513. [Crossref]
34. Pérez, P.; Domingo, L. R.; Aizman, A.; Contreras, R.; *Theor. Comput. Chem.* **2007**, *19*, 139. [Crossref]
35. Kujawski, J.; Czaja, K.; Jodłowska, E.; Dettlaff, K.; Politańska, M.; Żwawiak, J.; Kujawski, R.; Ratajczak, T.; Chmielewski, M. K.; Bernard, M. K.; *J. Mol. Struct.* **2016**, *1119*, 250. [Crossref]
36. Ekiert, R. J.; Krzek, J.; Rzeszutko, W.; *Chromatographia* **2008**, *67*, 995. [Crossref]
37. *Farmacopea Argentina, Monografías de Materia Prima*, 7th ed., vol. II; Administración Nacional de Medicamentos, Alimentos y Tecnología Médica, 2003. [Link] accessed in March 2023
38. *Farmacopea Argentina, Consideraciones Generales, Métodos Generales de Análisis*, 7th ed., vol. I; Textos de Información General Administración Nacional de Medicamentos, Alimentos y Tecnología Médica, 2003. [Link] accessed in March 2023
39. Homocianu, M.; *Microchem. J.* **2021**, *161*, 105797. [Crossref]

40. Catalán, J.; López, V.; Pérez, P.; *Liebigs Ann.* **1995**, *1995*, 793. [Crossref]
41. Laurence, C.; Legros, J.; Chantzis, A.; Planchat, A.; Jacquemin, D.; *J. Phys. Chem. B* **2015**, *119*, 3174. [Crossref]
42. Kamlet, M. J.; Doherty, R.; Taft, R. W.; Abraham, M. H.; *J. Am. Chem. Soc.* **1983**, *105*, 6741. [Crossref]
43. Taft, R. W.; Kamlet, M. J.; *J. Am. Chem. Soc.* **1976**, *98*, 2886. [Crossref]
44. Sancho, M. I.; Almandoz, M. C.; Blanco, S. E.; Castro, E. A.; *Int. J. Mol. Sci.* **2011**, *12*, 8895. [Crossref]
45. Reta, M. R.; Cartana, R.; Anunziata, J. D.; Silber, J. J.; *Spectrochim. Acta, Part A* **1993**, *49*, 903. [Crossref]
46. Kamlet, M. J.; Abboud, J. L. M.; Abraham, M. H.; Taft, R. W.; *J. Org. Chem.* **1983**, *48*, 2877. [Crossref]
47. Catalán, J.; *J. Phys. Chem. B* **2009**, *113*, 5951. [Crossref]
48. Nielsen, A. B.; Holder, A. J.; *Gauss View*, 5.0; Gaussian Inc., Pittsburgh, 2009.
49. Frisch, M. J.; Trucks, G. W.; Schlegel, H. B.; Scuseria, G. E.; Robb, M. A.; Cheeseman, J. R.; Scalmani, G.; Barone, V.; Mennucci, B.; Petersson, G. A.; Nakatsuji, H.; Caricato, M.; Li, X.; Hratchian, H. P.; Izmaylov, A. F.; Bloino, J.; Zheng, G.; Sonnenberg, J. L.; Hada, M.; Ehara, M.; Toyota, K.; Fukuda, R.; Hasegawa, J.; Ishida, M.; Nakajima, T.; Honda, Y.; Kitao, O.; Nakai, H.; Vreven, T.; Montgomery Jr., J. A.; Peralta, J. E.; Ogliaro, F.; Bearpark, M. J.; Heyd, J.; Brothers, E. N.; Kudin, K. N.; Staroverov, V. N.; Kobayashi, R.; Normand, J.; Raghavachari, K.; Rendell, A. P.; Burant, J. C.; Iyengar, S. S.; Tomasi, J.; Cossi, M.; Rega, N.; Millam, N. J.; Klene, M.; Knox, J. E.; Cross, J. B.; Bakken, V.; Adamo, C.; Jaramillo, J.; Gomperts, R.; Stratmann, R. E.; Yazyev, O.; Austin, A. J.; Cammi, R.; Pomelli, C.; Ochterski, J. W.; Martin, R. L.; Morokuma, K.; Zakrzewski, V. G.; Voth, G. A.; Salvador, P.; Dannenberg, J. J.; Dapprich, S.; Daniels, A. D.; Farkas, Ö.; Foresman, J. B.; Ortiz, J. V.; Cioslowski, J.; Fox, D. J.; *Gaussian 09*; Gaussian, Inc., Wallingford, CT, USA, 2009.
50. Balzani, V.; Ceroni, P.; Juris, A.; *Photochemistry and Photophysics: Concepts, Research, Applications*; Wiley-VCH Verlag GmbH & Co. KGaA: Weinheim, Germany, 2014, ch. 2, 3.
51. Evans, R. C.; Douglas, P.; Burrows, H. D.; In *Applied Photochemistry*; Evans, R. C.; Douglas, P.; Burrows, H. D., eds.; Springer: New York, 2013, ch. 1.
52. Reichardt, C.; Welton, T.; *Solvents and Solvent Effects in Organic Chemistry*, 4th ed.; Wiley-VCH Verlag GmbH & Co. KGaA: Germany, 2011, ch. 5, 6, 7.
53. Homocianu, M.; Airinei, A.; *J. Mol. Liq.* **2017**, *225*, 869. [Crossref]
54. Wermuth, C. G.; Ganellin, C. R.; Lindberg, P.; Mitscher, L. A.; *Pure Appl. Chem.* **1998**, *70*, 1129. [Crossref]
55. Griffith, R. K. In *Foye's Principles of Medicinal Chemistry*; Roche, V. F.; Zito, S. W.; Lemke, T. L.; Williams, D. A., eds.; Wolters Kluwer: USA, 2020, ch. 31.
56. Ji, H.; Zhang, W.; Zhou, Y.; Zhang, M.; Zhu, J.; Song, Y.; Lü, J.; Zhu, J.; *J. Med. Chem.* **2000**, *43*, 2493. [Crossref]
57. Sagatova, A. A.; Keniya, M. V.; Wilson, R. K.; Monk, B. C.; Tyndall, J. D. A.; *Antimicrob. Agents Chemother.* **2015**, *59*, 4982. [Crossref]

Submitted: November 17, 2022
Published online: April 11, 2023

